Surface-Micromachined Capacitive RF Switches With Low Actuation Voltage and Steady Contact

Sudhanshu Shekhar, K. J. Vinoy, *Member, IEEE*, and G. K. Ananthasuresh

***Abstract*— In this paper, we report fabrication and dynamic characterization of low-actuation-voltage capacitive radio frequency microelectromechanical systems (RF MEMS) switches with improved electromechanical performance. Electromechanical and electromagnetic modeling is used to modify the previously known geometries of switches and the number and size of holes in them to improve their overall dynamic characteristics. The switches are fabricated on a Pyrex glass substrate using a low-complexity four-mask surface micromachining process. These designs of MEMS switches require only 4.8–6.2 V as pull-in voltage. The dynamic behavior of these MEMS switches is investigated experimentally. Measured mechanical resonant frequency and quality factor are found to be in the range of 7.56–10.7 kHz and 1.1 to 1.2, respectively. Measured switching times for all the designs are 33–37 μs at their respective pull-in voltages. These switches show bounce-free switching during contact and fast settling after release. Two of the switch designs have insertion loss of less than 0.25 and 0.7 dB at 20 and 40 GHz, and isolation better than 30 dB. Close agreement between experimentally measured and simulation results demonstrates successful realization of fast-switching capacitive RF MEMS switches at low voltage.**

[2016-0152]

***Index Terms*— Capacitive switch, microelectromechanical systems (MEMS) switch, radio frequency MEMS (RF MEMS), release time, switching time, switching dynamics.**

I. Introduction

ADVANCES in microfabrication processes along with the design and modeling in the past three decades have shown that radio frequency microelectromechanical systems (RF MEMS) switches emerge as an attractive alternative for the existing semiconductor switches. RF MEMS switches are promising basic building blocks of the present and future communication systems including mobile phones, satellite communications, and defense as well as in high-end applications such as automated measurement and test equipment. RF MEMS switches can be metal-to-metal contact or capacitive in series or shunt configurations. Capacitive MEMS switches are preferred over the DC-contact switches as these provide very low insertion loss and high isolation at very high frequencies exceeding 10 GHz [1].

Manuscript received July 2, 2016; revised February 14, 2017; accepted March 8, 2017. Date of publication April 13, 2017; date of current version May 31, 2017. Subject Editor M. Rais-Zadeh. *(Corresponding author: Sudhanshu Shekhar.)*

S. Shekhar and K. J. Vinoy are with the Department of Electrical Communication Engineering, Indian Institute of Science, Bengaluru 560012, India (e-mail: sshekhar@ece.iisc.ernet.in; kjvinoy@ece.iisc.ernet.in).

G. K. Ananthasuresh is with the Department of Mechanical Engineering, Indian Institute of Science, Bengaluru 560012, India (e-mail: suresh@mecheng.iisc.ernet.in).

Color versions of one or more of the figures in this paper are available online at http://ieeexplore.ieee.org.

Digital Object Identifier 10.1109/JMEMS.2017.2688519

Despite their promising features, RF MEMS switches are yet to compete in the market due to their poor reliability. High actuation voltage generates high electric field between the switch electrodes that results in tunneling of charges into the dielectric causing stiction. The erratic behavior of dielectric due to high actuation voltage limits the lifetime and hence the reliability of MEMS switches [2]–[7]. In addition, high actuation voltage imparts large kinetic energy to the movable beam leading to the mechanical failure due to high impact force during the contact. Another drawback of high actuation-voltage is seen in the form of rebounds that happen due to high impact during the contact with the actuation electrode. Efforts have been made in the past to realize soft-landing, i.e., to reduce the impact force during the contact using tailored actuation pulse to achieve high reliability for MEMS switches [8]–[16]. Therefore, reduced bouncing during switching and fast settling upon release are other aspects of designing RF MEMS switches. Several applications (e.g., phased array antennas, adjustable LTE antennas, grating light valves (GLVs)) require bounce-free switching and fast-settling switches at low electrostatic actuation voltage [17]–[19]. Low-voltage MEMS switches are reported in the past [20]–[24]. However, low actuation voltage results in slow switching speed necessitating high actuation voltage [25]–[32].

The principal objective of this work is to realize MEMS switches with low actuation voltage without compromising on their RF and dynamic performance. In this work, we present three designs to realize capacitive MEMS switches. These switches are implemented in shunt configuration. A capacitive shunt switch results in low insertion loss in up-state (or un-actuated position) and high isolation in down-state (or actuated position). The switch topologies considered appear similar to some of the conventional designs [1]. However, their geometrical parameters including size and number of holes are modified to improve the pull-in voltage, switching dynamics, and RF performance. In the present work, detailed discussion on the mechanical aspects such as switching time, release time, smooth landing during the contact, and reduced oscillation after release are presented. The dynamic behavior along with RF performance such as insertion loss and isolation of all three designs are demonstrated experimentally. A comparative result based on dynamic performance is also highlighted to show that reported MEMS switches exhibit superior timing performance at low voltage as compared to MEMS switches reported in the past.

The organization of the paper is as follows: Section II presents design strategy and finite element analysis (FEA) of three switch topologies. In Section III, surface micromachining

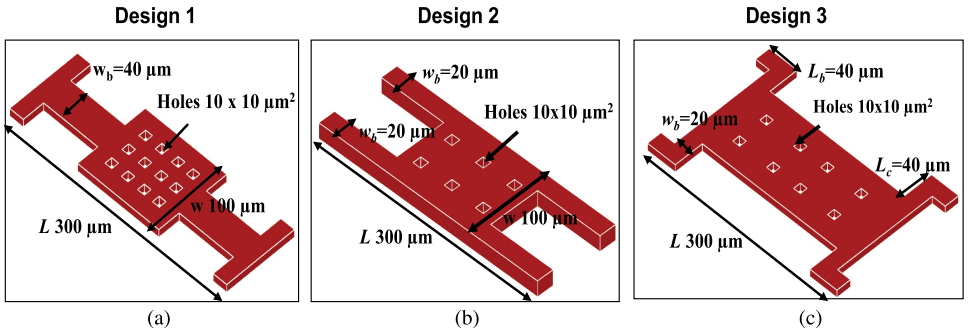

Fig. 1. Schematics of three designs of capacitive RF MEMS switches. (a) Design 1: T-support, (b) Design 2: parallel-support, and (c) Design 3: L-support beams.

approach used for the fabrication is described. In order to quantify the RF performance of fabricated MEMS switches, RF measurements are noted in Section IV. Mechanical characterization is performed to investigate the dynamic performance. The dynamic measurement results of the fabricated devices are discussed in Section V. Finally, in Section VI, discussion and conclusions drawn from the present work are included.

II. Design and Electromechanical Modeling of Switches

The switching action in a capacitive shunt RF MEMS switch is achieved by altering the capacitance between the switch beam and the signal line. The required electric potential needed for actuation is applied between the movable part and the signal line to vary the capacitance. A dielectric layer is included above the bottom electrode to avoid short circuit.

The geometry of the switch beam is pivotal to improve electromechanical performance in terms of its switching dynamics and RF performance. In order to realize an RF MEMS switch with low actuation voltage, the movable beam should have low spring constant, k, and the air-gap between the beam and the signal beneath it should be small. Low spring constant requires the switch beam to be thin. However, it should be thick as well as stiff enough to generate adequate restoring force in order to retain its original (un-deflected state) position once the external electrostatic force is removed. Various combinations of support-beams are attached to the central part of the switch membrane to investigate their mechanical flexibility.

A. Design

The three simple geometrical configurations considered in this work are shown in Fig. 1. The analytical expressions for the spring constants, k, for switch geometries described above are given by [1]:

For design 1:

$$k_{\text{eff}} = 2Ew\left(\frac{t}{L_b}\right)^3 \tag{1}$$

For design 2:

$$k_{\text{eff}} = 4Ew\left(\frac{t}{L_b}\right)^3 \tag{2}$$

For design 3:

$$k_{\text{eff}} = \frac{4Ew(t/L_b)^3}{1+(L_b/L_c)[(L_b/L_c)^2+12\frac{(1+\upsilon)}{(1+(w/t)^2)}]} \tag{3}$$

where E is the Young's modulus, υ the Poisson's ratio, w the beam width, t the beam thickness, and L_b and L_c are lengths of beam segments. To investigate electromechanical properties such as stiffness, pull-in voltages, and RF characteristics, FEM simulations on these proposed switch designs are performed. Simulation results are presented in Section II D.

B. Effect of Beam Thickness on Switch Dynamics

One dimensional (1-D) model, although not very accurate, can be used for understanding the dynamic behavior of MEMS switches. A 1-D model treats the MEMS switch as a lumped mass and spring system [33]. The switching and the release times can be obtained from the dynamic equation of motion with and without actuation:

$$m\frac{d^2x}{dt^2}+b\frac{dx}{dt}+kx = F_e = \frac{1}{2}\frac{\epsilon_0 A {V_s}^2}{(g_0-x)^2} \tag{4}$$

$$m\frac{d^2x}{dt^2}+b\frac{dx}{dt}+kx = 0 \tag{5}$$

where F_e is the electrostatic force, m is the effective-mass, b is the damping coefficient, k is the stiffness of the beam, V_s is the actuation voltage, and g_0 is the initial gap (when $V_s = 0$).

The switching time or pull-in time is defined as the time taken by the movable beam to reach the dielectric layer whereas the time required by the beam to traverse within 10% of the original gap, g_0, after the removal of actuation voltage, is defined as the release time (or pull-up time). After modifying Eq. 4 for the case of no-damping (i.e., $b = 0$), with initial conditions i.e., $x = 0$ and $\frac{dx}{dt} = 0$ at $t = 0$, the analytical expressions for switching and release times are derived. It may be noted that the dynamic equation of motion (Eq. 4) is a nonlinear second-order differential equation and the closed-form solutions for switching and release times are difficult without assuming zero damping. This simplified analysis without damping, though not very accurate, helps in understanding the dynamic behavior theoretically. The derived

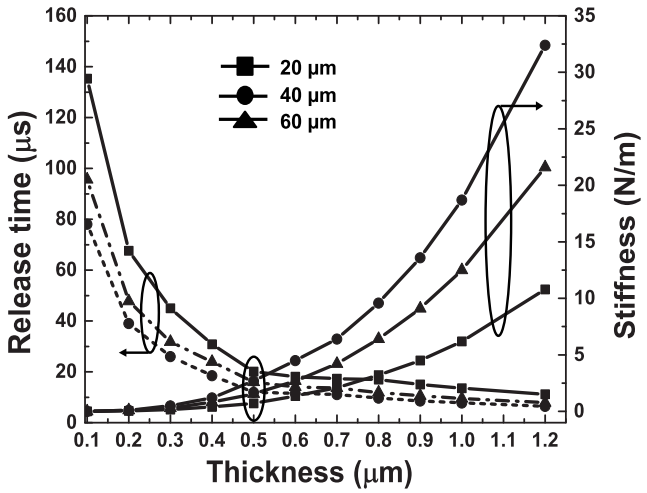

Fig. 2. Release time and stiffness as a function of thickness for different values of beam width, w_b.

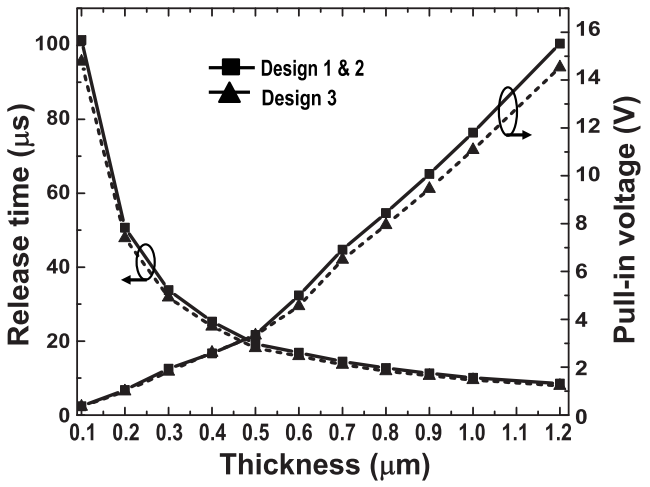

Fig. 3. Release time and pull-in voltage as a function of thickness of switch beams.

expressions for switching and release time are given by [34]:

$$t_{pi} = \int_0^{g_0} \frac{1}{\sqrt{\frac{\epsilon_0 A V_s^2}{m(g_0 - x)} - \frac{k}{m}x^2 - \frac{\epsilon_0 A V_s^2}{m g_0}}} dx \tag{6}$$

From the derived closed-form expression of the switching time, t_{pi}, (Eq. 6), it is evident that the switching time is inversely proportional to the actuation voltage. Therefore, we see that the switching time of a MEMS switch can be made faster by applying actuation voltage, V_s, 1.2 to 1.4 times higher than the actual V_{PI}. However, release happens entirely due to its mechanical restoring force when the applied external electrostatic force, $F_e = 0$ and the switch retains its undeflected position. The release time is expressed as [34]:

$$t_{pu} = \frac{1}{4 f_0} = \frac{\pi}{2}\sqrt{\frac{m}{k}} \tag{7}$$

where, t_{pu} is defined as the release time or pull-up time when the actuation voltage is turned off (i.e., when $V_s = 0$).

The preceding result (Eq. 7) is not surprising because the electrode moves a quarter of its cyclical motion to reach the un-deformed state for the first time. Consequently, the switch response time, upon release, for a flexible structure is more as compared to stiff structures. Therefore, switch geometry should pose sufficient restoring force. The stiffness, k, can be lowered by reducing the switch beam thickness as well as increasing the beam flexibility using support beams. However, low-k results in low mechanical restoring force as

$$F_{restoring} = k(g_0 - g) = kx \tag{8}$$

where, g_0 and g are the heights of the switch beam in un-deformed and deformed states.

Fig. 2 presents the dynamic response along with parameters such as stiffness and beam thickness. The release response time for a 0.3 μm thick switch is found to be almost 60% more compared to the release response time for a 0.5 μm thick switch. Fig. 3 shows pull-in voltage and release time as a function of the beam thickness of different switch topologies. The optimum thickness (0.5 μm) and the beam width, w_b, (40 μm for design 1 and 20 μm for designs 2 and 3, respectively) for the device is decided based on the dynamic response. The dynamic simulation results ensure that reasonably fast release ($<$ 20 μs) for a MEMS switch of thickness 0.5 μm can be achieved at low actuation voltage ($<$ 6 V). The electromechanical and dynamic behavior of MEMS switches are studied using FEA-based MEMS simulator (CoventorWare).

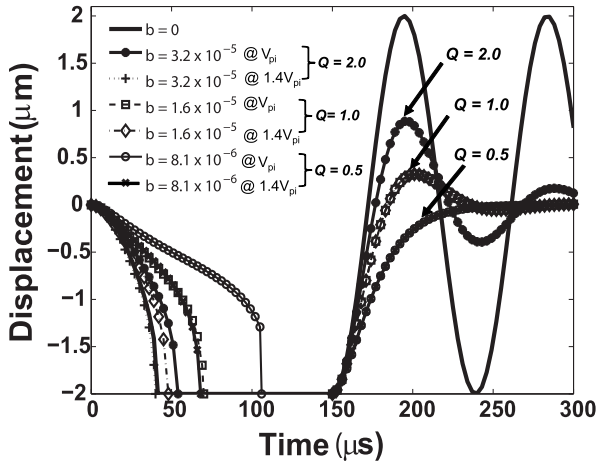

Fig. 4. Simulated switching and release time response for different values of Q-factor at different actuation voltages.

C. Incorporation of Holes in the Switch

To estimate the switching dynamics as mentioned in the previous section, certain assumptions such as $b = 0$ are needed. However, the air damping influences micro-structures (cantilever, fixed-fixed beams) used to realize MEMS switches. The switch dynamics can be improved by introducing holes in the structural layer by reducing the squeeze-film damping.

Fig. 4 illustrates switching and release response times as a function of damping coefficient, b and the corresponding Q-factor. We note that for low-damping (i.e., $b \leqslant 1 \times 10^{-6}$), the switch exhibits under-damped oscillation whereas

without damping (i.e., $b = 0$), the switch continues oscillating. The influence of high value of damping coefficient (i.e., $b \geqslant 1 \times 10^{-4}$) on the switching as well as release times are also investigated. High actuation voltage ($V_s > V_{PI}$) is required in such cases. From the simulated results shown in Fig. 4, it is evident that the effect of damping is very much prevalent on the release time as compared to the switching time [1], [13], [16], [21].

We note that, it takes more than 200 μs for the switch to settle for $Q = 2.0$, whereas switch is stabilized within 100 μs and 50 μs for $Q = 1.0$ and $Q = 0.5$, respectively. We note that low Q results in fast settling due to suppressed oscillation and slow release time when the actuation voltage, $V_s = V_{PI}$. As noted earlier, the oscillations after release i.e., when $V_s = 0$, is undesirable in many applications as these oscillations can modulate the RF signal flowing through the transmission line. To eliminate bouncing during contact and the oscillations after release, strategies such as command wave shaping techniques have been proposed [10], [35]–[37].

Furthermore, the influence of squeeze-film damping on the switching time cannot be neglected. However, the effect can be mitigated by applying voltage higher than the pull-in voltage ($V_s > V_{PI}$). Therefore, the dynamic response of MEMS switches are studied under two different conditions: (i) $V_s = V_{PI}$ and (ii) $V_s = 1.4\ V_{PI}$. We note that the effect of high actuation voltage, V_s, on the release response is insignificant as compared to the switching time (see Fig. 4). Release response for $V_s = V_{PI}$ and $V_s = 1.4\ V_{PI}$ overlap except for the case when $b = 0$, while switching time reduces to almost half when the actuation voltage, $V_s = 1.4\ V_{PI}$. From the results presented in Fig. 4, we conclude that the switching dynamics is governed by the quality factor, Q, which is further related to the air damping. A high quality factor indicates low loss due to damping. It is generally understood that a MEMS switch with $Q < 1.0$ results in low switching time while $Q > 2.0$ results in long settling time [21], where the settling time is defined as the time taken by the switch to settle within 5% of original gap. The results presented in Fig. 4, also confirms that low-Q switches have suppressed oscillation after the release.

Therefore, the design strategy followed in our work is to introduce holes in the switch membrane. The presence of holes reduces the squeeze-film damping and also helps in achieving the required Q for suppressed oscillation after the release. The quality factor, Q, is estimated using $Q = k/(\omega_0 b)$, where b is the damping coefficient given by [1]:

$$b = \frac{12}{N\pi}\frac{\mu A^2}{g_0^3}\left(\frac{p}{2} - \frac{p^2}{8} - \frac{1n(p)}{4} - \frac{3}{8}\right) \tag{9}$$

where N is the number of holes, μ is the coefficient of viscosity, and p is the total area covered by the holes. These holes reduce squeeze-film damping by allowing the underneath air to escape and thus improve the switching dynamics. It also helps in facilitating under etching of the sacrificial layer underneath. Therefore, we see that the number and size of holes in the switch beam is crucial. Table I summarizes the change in Q value for different number of holes in the structural layer. The numbers in bold letters correspond to the number of holes used in the switch topologies considered in the present work. The other aspect of holes in switch membrane can be seen on the RF performance. The reduction in the number of holes ensures a large effective capacitive area that improves the isolation of capacitive MEMS switches in the down-state or actuated position. However, the effect of holes is insignificant on the up-state capacitance [1]. Therefore, considering aforementioned facts, all the switch topologies are incorporated with fewer holes with adequate size ($10 \times 10\ \mu m^2$) that covers less than 10% of the actuation electrode area, A. This approach also helps in achieving low Q (~ 1) for all the switch topologies.

TABLE I
EFFECT OF HOLES ON QUALITY FACTOR

Hole mesh (number of holes)	Quality factor, Q	
	Design 1, 2	Design 3
5 × 6 (30)	21.0	46.0
4 × 5 (20)	8.13	18.0
3 × 4 (12)	2.99	6.68
2 × 4 (8)	1.48	3.32
3 × 3 (9)	**1.81**	4.04
2 × 3 (6)	**0.93**	2.09
2 × 2 (4)	0.5	**1.13**

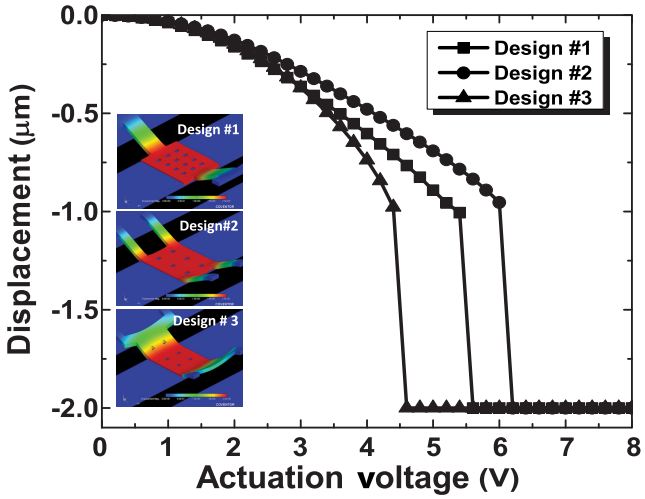

Fig. 5. Simulated pull-in voltage of various switch geometries.

D. FEA Modeling

The FEA-based electromechanical simulation results are shown in Fig. 5. The simulated pull-in voltages for these designs are 5.5 V (design 1), 6.3 V (design 2), and 4.5 V (design 3), respectively. These switch designs result in $k = 1.56$ N/m for design 1 and 2, and $k = 1.34$ N/m for design 3. The FEA analysis results show contact force of $> 50\ \mu$N and $> 100\ \mu$N at V_{PI} and $1.5\ V_{PI}$ respectively for all the designs whereas restoring forces of 34.1 μN, 37.3 μN, and 27.4 μN, is estimated for design 1, 2 and 3, respectively.

To quantify the effect of geometrical parameters, dielectric material and its thickness on the RF performance, all the proposed switch topologies were modeled using Ansoft HFSS

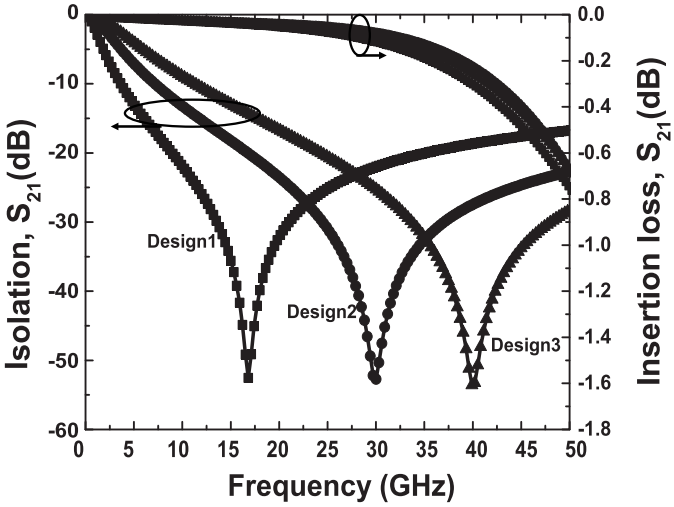

Fig. 6. Simulated S-parameters of various switch topologies in up-state (insertion loss) and down-state (isolation) positions.

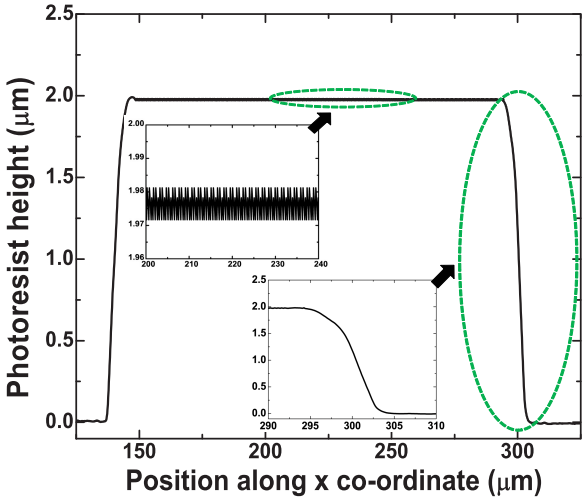

Fig. 7. Surface profilometer measured step height (thickness) of the photo-resist.

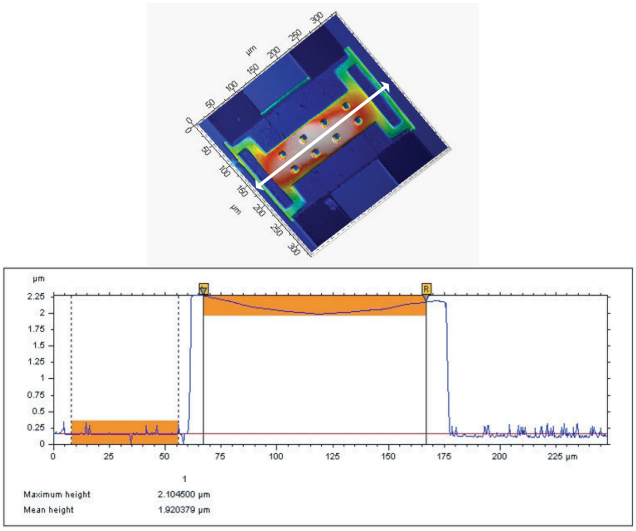

Fig. 8. Optical interferometer results showing switch profile and flatness.

(High Frequency Structure Simulator) which is a FEA-based full-wave electromagnetic software. The switch is suspended over a 80 μm/120 μm/80 μm coplanar wave guide (CPW) transmission line. A 50 Ω transmission line, for a physical length and thickness of 800 μm and 0.5 μm, is realized using the slot-width and the signal-width of 80 μm and 120 μm, respectively. The simulation results show the characteristic impedance, Z_0, of the CPW transmission line from 50.4 Ω to 51.2 Ω in the frequency range up to 60 GHz.

The support-beam width, w_b, is varied from 20 μm to 40 μm to estimate the loss. We note that the insertion loss is least affected due to the beam-width variation. However, drop in isolation as well as slight shift in the electrical resonance frequency is noticeable.

There is trade-off between the gap of the switch and the RF performance: small gap between the switch membrane and the fixed bottom electrode deteriorates the isolation characteristics. The optimized switch topologies for a gap of 2 μm exhibit good RF performance in terms of return loss, insertion loss, and the isolation as shown in Fig. 6. Extensive FEA simulations are performed on these designs before fabrication. Proposed switch topologies result in improved electromechanical and RF performances. More details on the dynamic behavior and RF performance along with experimental results are discussed in Section IV and V.

III. Fabrication

The MEMS switches presented in this paper are fabricated on a 4″ Pyrex glass substrate using surface micromachining [38]. A 500 μm thick Pyrex glass is used as a substrate because of its excellent electrical and RF response at high frequencies. The CPW transmission lines are fabricated by sputtering a thin layer of Cr/Au/Cr (10 nm/100 nm/10 nm). A 1500 Å thick silicon nitride (Si_3N_4) is used as the dielectric material. Later, the deposited Si_3N_4 is pattered to act as a passivization layer between the switch membrane and the signal line. The measured step height of the deposited dielectric is found to be in the range of 1520-1550 Å, which is close to the target value of 1500 Å. The surface roughness is also measured using an Atomic Force Microscope (AFM - Bruker Dimension Icon) and found to be < 5 nm.

A positive photoresist (PPR) Shipley 1813 is used as the sacrificial layer. Sacrificial layer's thickness provides the required air-gap between the movable and fixed signal line of the switch. The target gap height is 2 μm. To achieve the required thickness; PR is spin coated at the speed of 2000 rpm for 30s followed by soft baking at 90°C for 60s. The sacrificial layer is then patterned and hard baked at 120°C. Pre-bake and post-bake of sacrificial is optimized to get a planar surface and rounded edge profile. To ensure the height of the sacrificial layer, after the hard bake, Dektak surface profilometer is used. The PR step height (thickness) is shown in Fig. 7. The measurement results show the step height of the sacrificial layer as 1.97 - 1.98 μm with surface roughness of 10 nm. We also note that a round edge profile is achieved with the aforementioned spin speed and post-bake process. They are highlighted by dotted ovals in the inset picture in Fig. 7. This rounded edge profile helped us to eliminate the

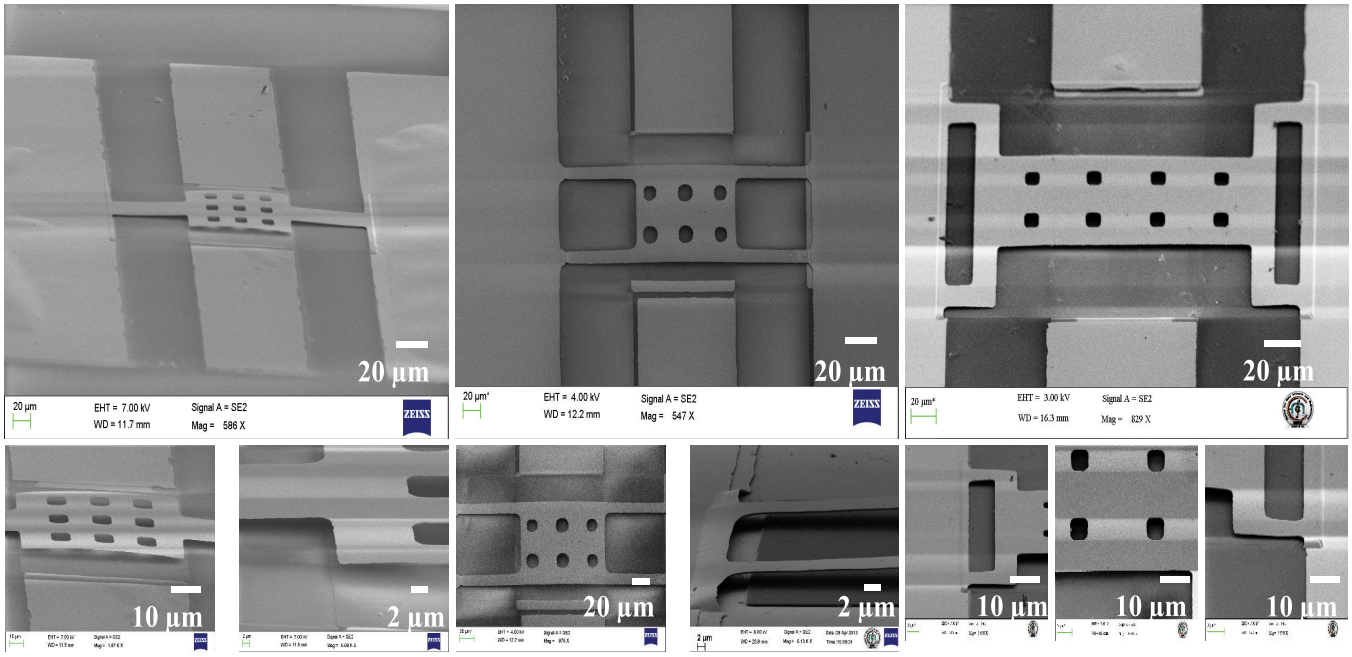

Fig. 9. SEM images of fabricated RF MEMS switches.

extra photolithography step of creating metal post as an anchor. Thus the whole fabrication process is restricted to four-masks only.

A 0.5 μm thick fil of Au is then sputtered and patterned as a structural layer. Holes of 10×10 μm^2 are formed in the central part of the switch to facilitate under etching during the sacrificial release. As discussed in Section II, this design for holes is used to ensure the required dynamic response for the switch. Dry release using reactive ion etching (RIE) is an alternate of sacrificial layer removal where O_2 plasma is used to ash-out the PR. However, thin-metal film cannot handle very high RF-power as the RIE done at high RF-power develops residual stress in the thin-metal membrane. Therefore, CO_2 critical point dryer (CPD) is used to realize stiction-free microstructures.

The released height of the switch is measured using an optical interferometer (Taylor Hobson PRECISION with Talysurf CCI). The gap height is measured to be 2.10 μm and flatness measurement results show the deflection in the range of 100 nm (Fig. 8). The final realized thickness of the conductors is 0.6 μm. Based on the measured results, the overall process tolerance is estimated to be within $\pm$ 0.3 μm. All the proposed switch designs are fabricated on the same wafer. Fig. 9 presents the scanning electron microscope (SEM) images of released RF MEMS switches.

IV. RF Characterization

Agilent E8361A Vector Network Analyzer (VNA) with 200 μm pitch coplanar probes is used to measure S-parameters to quantify the performance of the fabricated RF MEMS switches. All the on-wafer measurements were performed using Short-Open-Load-Thru (SOLT) calibration technique in the frequency range up to 50 GHz under normal atmospheric conditions. The insertion loss in up-state is found to be less than 0.25 dB and 0.7 dB at 20 GHz and 40 GHz, respectively for designs 2 and 3, whereas for design 1 it is measured to be 1 dB at 20 GHz. The measured isolation in the down-state position is found to be better than 30 dB for design 1 (at 17 GHz) and better than 40 dB for design 2 (at 30 GHz) and 3 (at 40 GHz), respectively. The up- and down-state positions have been defined as un-actuated (when $V_s = 0$) and actuated ($V_s = V_{PI}$) conditions of the MEMS switch.

Fig. 10 presents measured and simulated S-parameters in up and down-state positions of one of the switch designs proposed in this work (design 2). Measurement results of rest of the designs also compared with the simulation results and a close agreement is reported. These RF MEMS switches are tested for input RF power of 1 μW to a maximum of 1 mW (in the frequency range up to 40 GHz). Measured RF response was found to be in good agreement with the simulated results as evident from the comparison results.

V. Dynamic Characterizations

A. Resonant Frequency and Q-factor Measurements

Mechanically movable micro-structures are the crucial parts of RF MEMS switches. These micro-structures are found to have different effects on the switching dynamic in terms of switching and release time response. The two main factors that affect switching dynamics are the stiffness, k, and the quality factor, Q. A Laser Doppler Vibrometer (LDV), PolyTech MSA-500, was used for the extraction of mechanical resonant frequency, f_0, and the quality factor, Q, of fabricated MEMS switches. The mechanical resonance frequency, f_0, associated with the mass, m, and the stiffness, k, of the beam is given by Eq. 7 ($f_0 = 1/2\pi\sqrt{k/m}$), as explained in Section II.

Fig. 11 presents the mechanical resonant frequency response of parallel-support MEMS switch (design 2) using

TABLE II
SIMULATED AND MEASURED DYNAMIC CHARACTERISTICS OF FABRICATED MEMS SWITCHES

Switch Design	FEM		Measured	
	V_{PI}(V)	$f_0(kHz)$	V_{PI}(V)	$f_0(kHz)$
Design 1	5.5	7.61	5.4	7.56
Design 2	6.3	9.35	6.2	10.7
Design 3	4.5	8.29	4.8	8.35

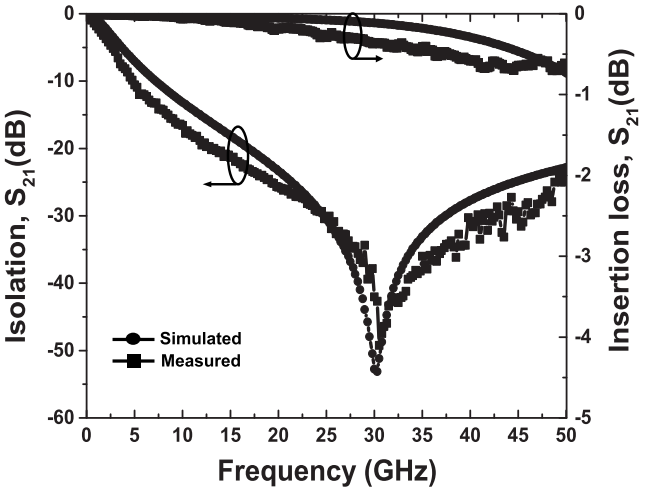

Fig. 10. Comparison of simulated and measured *S*-parameters in up-state (insertion loss) and down-state (isolation) of switch design 2.

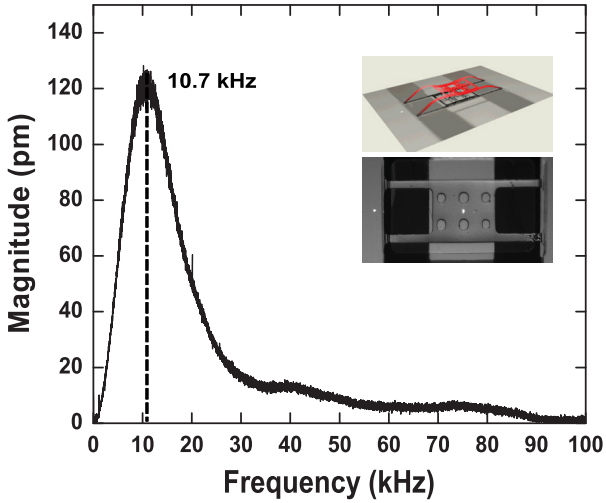

Fig. 11. Mechanical resonant frequency response of parallel-support (design 2) captured using LDV.

LDV. The amplitude-frequency response is measured using a combination of 0.6 V AC and 2 V DC signals. The inset pictures (Fig. 11) show the optical micrographs and the LDV-constructed motion images of the switch. The measurements were conducted under standard temperature (25°C) and normal pressure (101 kPa) conditions. Table II summarizes simulated and measured results. The minor discrepancy between these results indicates good fabrication control.

The Q-factor plays a very important role in evaluating switching and release dynamics of a MEMS switch.

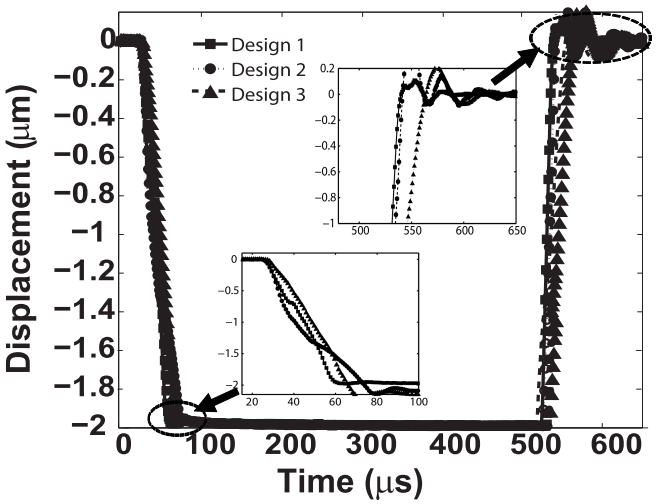

Fig. 12. Measured switching and release times of various switch designs using LDV.

The details on switching dynamics as function of Q-factor can be found in Section II C. The Q-factor is a measure of the sharpness of the resonant peak and is calculated using the following formula:

$$Q = \frac{f_{\text{res}}}{f_1 - f_2} \tag{10}$$

where f_{res} is the resonance frequency and $(f_1 - f_2)$ is the half-power bandwidth.

We used half-power point method to evaluate the Q-factor. The experimental amplitude-frequency curve is extracted using LDV. Similar approach is used for the rest of switch designs. The measured Q-factor was found to be in between 1.1 to 1.2 for all the three designs. A Q-factor for the best release response is approximately 1.0. This value as explained earlier in Section II C, ensures reasonably fast switching with small settling time. The measured results reported in this work were comparable to the recommended value of Q.

B. Switching and Release Time Measurements

Fig. 12 presents the dynamic measurement results. LDV is used for the measurement of switching and release times of realized MEMS switches. The dynamic behavior of these switches were monitored by providing a train of square pulse voltage along with proper offset voltage level. Measurements were performed under normal atmospheric conditions. A square actuation pulse signal of cyclic frequency 1 kHz with 50% duty cycle was used. Since, these switches need low voltage (< 10 V) for actuation, the amplitude of the square wave was varied from 4.0 V to 7.0 V in steps of 200 mV to measure switching and release times.

Smooth-landing of the switch membrane (no ripples) during the contact and suppressed oscillations, after the release, is evident from the measured results. We observed that these switches not only show fast settling time but also reduced bouncing of the switch membrane during the contact. During small settling, the displacement amplitude stays within 5% of the initial gap, g_0. They are highlighted by dotted ovals in the

TABLE III
MEASURED SWITCHING TIMES AT DIFFERENT ACTUATION VOLTAGES

Switch Design	Measured switching time(μs)		
	@V_{PI} (V)	@1.2 V_{PI} (V)	@ 1.4V_{PI} (V)
Design 1	36	28	12
Design 2	37	21	14
Design 3	33	31	18

inset picture in Fig. 12. Measurement results suggest that the bouncing of the switch membrane after the release i.e., when $V_s = 0$, can be further suppressed by applying low actuation voltage. Since, oscillations in the switch after release increases the overall settling time. Therefore, from the experimental results presented in this work, it may be concluded that the long settling time and the ripples during the contact, often considered as a drawback of many RF MEMS switches, have been overcome in the proposed switch topologies. This effect can be attributed to the low Q-factor and the low actuation voltage.

The switching time depends on the actuation voltage: the higher the actuation voltage the faster is the switching response. These switches were actuated even at higher potential for experimental verification. We noticed that for switch design 1, the switching time is reduced from 36 μs to 28 μs, when the actuation voltage i.e., V_s, is increased to 1.2 times the pull-in voltage, V_{PI}. Similar effect has been noticed for other switch designs. However, measured release times for all the MEMS switches were found to be less than 20 μs. Table III summarizes the experimentally measured switching time at different actuation voltages.

VI. DISCUSSION AND CONCLUSIONS

In this paper, design, fabrication, and dynamic characterization of capacitive RF MEMS switches are presented. Although most of the MEMS switches reported in the past show good RF performance, they have limitations in terms of either high actuation voltage or high switching time (or both). In order to achieve fast switching, the applied actuation voltage was usually very high. We compared the results obtained in the present work with published results. Fig. 13 presents a comparison of the switching time and the actuation voltage for all the switch designs (marked with blue triangles) along with those reported in recent years. The plotted result clearly shows that MEMS switches reported in this work are comparatively faster (at low-voltage). The measured results suggest that even a thin-metal membrane of 0.5 μm is sufficient to realize bounce-free, fast-switching capacitive RF MEMS switches with excellent RF and dynamic performances at low-voltage. Also, mechanically-flexible designs considered as switches proves the validity of approach in the realization of bounce-free fast settling MEMS switches at low-voltage. The reason for improved overall performance such as pull-in voltage, smooth switching, fast-settling upon release as well as better RF performance of MEMS switches in presented work can be attributed to the geometry, thickness, width of support-beams, and holes (number and size) in the switch membrane.

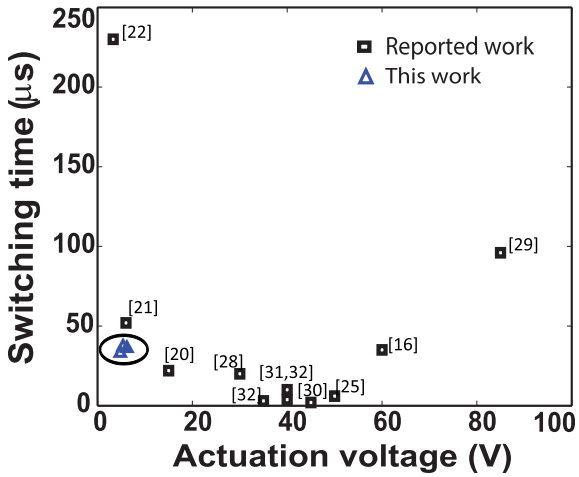

Fig. 13. Comparison of the switching time versus actuation voltage.

The introduction of each additional layer adds to the process complexity. The reason for selecting three designs is not only to achieve improved electromechanical and RF performances but also their process compatibility.

The measured RF performance, i.e., return loss better than 12 dB, insertion loss less than 0.7 dB (design 2 and 3) and isolation better than 30 dB (design 1) and 40 dB (design 2 and 3), in the frequency range up to 50 GHz, make the MEMS switches reported in this work a suitable choice for high frequency applications. A comparison between the measurement results obtained in this work and published results is presented in Table IV. The fabricated capacitive RF MEMS switches show comparable performance in terms of electrical and RF characteristics.

MEMS switches reported in this work need low voltage for actuation. These switches are fabricated using thin gold-film, which indicates that these switches cannot qualify for high-power applications. Based on theoretical calculations, the RF power at which self-actuation takes place for these switches is found to 0.5 - 0.98 W. However, VNA-based S-parameter measurement could be performed for a maximum input power of up to 0.5 mW due to limitations of the equipment.

The dynamic behavior of a MEMS switch is significantly influenced by the squeeze-film damping. By introducing holes in the structural layer squeeze-film effect can be mitigated. Since, the oscillations before it settles can modulate the power of input signal passing through the transmission line, a low Q-factor is recommended for RF MEMS switches. For Q-factor $\sim$ 1.0, the switch takes less time to settle as well as the overshoot is also reduced. Therefore, in our proposed switch designs, we introduced holes of 10×10 μm^2 in the switch membrane. The introduction of holes reduces the squeeze-film damping. Consequently, the dynamic performance of switches is improved. We note that the measured Q-factor of multiple switches reported in this work (1.1 to 1.2) is in satisfactory agreement with the recommended value i.e., $Q \approx 1$, for the best release response. The fast settling time reported in this work can be considered as a salient feature of these MEMS switches.

TABLE IV
COMPARISON OF CAPACITIVE RF MEMS SWITCHES WITH REPORTED MEMS SWITCHES

Ref.	Actuation mechanism	Switch beam material	Thickness (μm)	Actuation voltage (V)	Insertion loss (dB)	Isolation (dB)
6	Electrostatic	Au	1	15 - 20	0.2 @ 10 GHz; 0.8 @ 30 GHz	35 @ 23 GHz
20	Electrostatic	Au	-	< 15	0.1 @ 40 GHz	20 @ 40 GHz
22	Electro-magnetic	Au	1	5	0.85 @ 19.5 GHz	20.7 @ 19.5 GHz
23	Electro-magnetic	Au	3.6	4.3	0.52 - 2.05 @ 20 GHz	36 @ 20 GHz
25	Electrostatic	Al-alloy	-	50	0.14 @ 20 GHz; 0.25 @ 35 GHz	24 @ 20 GHz; 35 @ 35 GHz
29	Electrostatic	Al	-	82	0.98 @ 20 GHz	17.9 @ 20 GHz
31	Electrostatic	Ti/TiN	-	30	0.5 upto 140 GHz	15 @ 90 - 140 GHz
30, 32	Electrostatic	Au	> 7	35 - 45	0.7 @ 30 GHz	30 @ 30 GHz
This work	Electrostatic	Au	0.5	4.8 - 6.3	0.25 @ 20 GHz; 0.7 @ 50 GHz	30 - 40 @ 17; 30 @ 40 GHz

The mechanically-flexible structures fabricated using 0.5 μm thick-metal (gold) membrane show excellent dynamic performance: almost zero-bounce during the contact and low oscillation after the release which results in fast settling. Dynamic measurement results demonstrate that low-actuation results in reduced bouncing (during the contact). The electro-mechanical parameters such as pull-in voltage and mechanical resonance frequency predicted by FEA-based simulations are found to be in close agreement with experimental results (as shown in Table II). Reported MEMS switches need a voltage of 5.5 V, and 6.2 V, and 4.8 V for actuation. Similarly, the measured resonance frequencies are found to be 7.56 kHz (design 1), 10.7 kHz (design 2), and 8.35 kHz (design 3), respectively. Thus, there is about 0.65%, 0.7%, and 14% of discrepancy between the experimental and the computed natural frequency among measured devices. However, the discrepancy of 1.8%, 1.5%, and 6.6% in the pull-in voltages is found between calculated and experimental results for various switch topologies. The reason for such discrepancies may be minor geometrical variations and the residual stress induced during the fabrication.

Fabrication results are satisfactory and the variations as compared to the proposed designs are found to be insignificant. Based on the measured results, the overall process tolerance is estimated to be within ± 0.3 μm. Close agreement between the experimentally measured and the simulation results demonstrate successful realization of fast-switching capacitive RF MEMS switches at low-voltage with steady contact and better RF performance.

ACKNOWLEDGMENT

The reported MEMS devices were fabricated and characterized at the Centre for Nano Sciences and Engineering (CeNSE) at the Indian Institute of Science, Bengaluru. The authors would like to thank the facility technologists of CeNSE for their assistance in the fabrication and characterization.

REFERENCES

[1] G. M. Rebeiz, *RF MEMS: Theory, Design, and Technology*. Hoboken, NJ, USA: Wiley, 2003.

[2] J. Wibbeler, G. Pfeifer, and M. Hietschold, "Parasitic charging of dielectric surfaces in capacitive microelectromechanical systems (MEMS)," *Sens. Actuators A, Phys.*, vol. 71, no. 1, pp. 74–80, Nov. 1998.

[3] C. Goldsmith *et al.*, "Lifetime characterization of capacitive RF MEMS switches," in *IEEE MTT-S Int. Microw. Symp. Dig.*, vol. 1. May 2001, pp. 227–230.

[4] A. Tazzoli, V. Peretti, and G. Meneghesso, "Electrostatic discharge and cycling effects on ohmic and capacitive RF-MEMS switches," *IEEE Trans. Device Mater. Rel.*, vol. 7, no. 3, pp. 429–437, Sep. 2007.

[5] S. Mellé *et al.*, "Reliability modeling of capacitive RF MEMS," *IEEE Trans. Microw. Theory Techn.*, vol. 53, no. 11, pp. 3482–3488, Nov. 2005.

[6] A. Persano, A. Cola, G. De Angelis, A. Taurino, P. Siciliano, and F. Quaranta, "Capacitive RF MEMS switches with tantalum-based materials," *J. Microelectromech. Syst.*, vol. 20, no. 2, pp. 365–370, 2011.

[7] W. M. Van Spengen, "Capacitive RF MEMS switch dielectric charging and reliability: A critical review with recommendations," *J. Micromech. Microeng.*, vol. 22, no. 7, p. 074001, 2012.

[8] C. Goldsmith, D. Forehand, X.-B. Yuan, and J. Hwang, "Tailoring capacitive switch technology for reliable operation," in *Proc. Govt Microcircuit Appl. Critical Tech. Conf.*, 2006, pp. 1–4.

[9] D. A. Czaplewski *et al.*, "A soft-landing waveform for actuation of a single-pole single-throw ohmic RF MEMS switch," *J. Microelectromech. Syst.*, vol. 15, no. 6, pp. 1586–1594, Dec. 2006.

[10] V. Leus, A. Hirshberg, and D. Elata, "Optimizing the dynamic response of RF MEMS switches using tailored voltage pulses," in *Proc. Int. Conf. Thermal, Mech. Multi-Phys. Simul. Experim. Microelectron. Micro-Syst. (EuroSimE)*, Apr. 2007, pp. 1–4.

[11] M. Lishchynska, M. Cychowski, N. Canty, T. O'Mahony, and K. Delaney, "Optimising dynamic behaviour of electrostatically actuated MEMS contact switch," in *Proc. Int. Conf. Thermal, Mech. Multi-Phys. Simul. Experim. Microelectron. Micro-Syst. (EuroSimE)*, Apr. 2009, pp. 1–7.

[12] A. Jain, P. R. Nair, and M. A. Alam, "Strategies for dynamic soft-landing in capacitive microelectromechanical switches," *Appl. Phys. Lett.*, vol. 98, no. 23, p. 234104, 2011.

[13] K.-S. Ou, K.-S. Chen, T.-S. Yang, and S.-Y. Lee, "Fast positioning and impact minimizing of MEMS devices by suppression of motion-induced vibration by command-shaping method," *J. Microelectromech. Syst.*, vol. 20, no. 1, pp. 128–139, Feb. 2011.

[14] A. Persano, A. Tazzoli, A. Cola, P. Siciliano, G. Meneghesso, and F. Quaranta, "Reliability enhancement by suitable actuation waveforms for capacitive RF MEMS switches in III–V technology," *J. Microelectromech. Syst.*, vol. 21, no. 2, pp. 414–419, 2012.

[15] G. De Pasquale, M. Barbato, V. Giliberto, G. Meneghesso, and A. Somà, "Reliability improvement in microstructures by reducing the impact velocity through electrostatic force modulation," *Microelectron. Rel.*, vol. 52, nos. 9–10, pp. 1808–1811, 2012.

[16] J. Small, A. Fruehling, A. Garg, X. Liu, and D. Peroulis, "DC-dynamic biasing for >50× switching time improvement in severely underdamped fringing-field electrostatic MEMS actuators," *J. Micromech. Microeng.*, vol. 22, no. 12, p. 125029, 2012.
[17] G. M. Rebeiz and J. B. Muldavin, "RF MEMS switches and switch circuits," *IEEE Microw. Mag.*, vol. 2, no. 4, pp. 59–71, Dec. 2001.
[18] C. Siegel, V. Ziegler, C. von Wächter, B. Schönlinner, U. Prechtel, and H. Schumacher, "Switching speed analysis of low complexity RF-MEMS switches," in *Proc. German Microw. Conf. (GeMiC)*, 2006, pp. 28–30.
[19] B. Kim, M. C. Schmittdiel, F. L. Degertekin, and T. R. Kurfess, "Actively controlled diffraction grating interferometer MEMS devices," *Proc. SPIE*, vol. 5721, pp. 151–158, Feb. 2005.
[20] R. Chan, R. Lesnick, D. Becher, and M. Feng, "Low-actuation voltage RF MEMS shunt switch with cold switching lifetime of seven billion cycles," *J. Microelectromech. Syst.*, vol. 12, no. 5, pp. 713–719, Oct. 2003.
[21] D. Peroulis, S. P. Pacheco, K. Sarabandi, and L. P. B. Katehi, "Electromechanical considerations in developing low-voltage RF MEMS switches," *IEEE Trans. Microw. Theory Techn.*, vol. 51, no. 1, pp. 259–270, Jan. 2003.
[22] I.-J. Cho, T. Song, S.-H. Baek, and E. Yoon, "A low-voltage and low-power RF MEMS series and shunt switches actuated by combination of electromagnetic and electrostatic forces," *IEEE Trans. Microw. Theory Techn.*, vol. 53, no. 7, pp. 2450–2457, Jul. 2005.
[23] I.-J. Cho and E. Yoon, "Design and fabrication of a single membrane push-pull SPDT RF MEMS switch operated by electromagnetic actuation and electrostatic hold," *J. Micromech. Microeng.*, vol. 20, no. 3, p. 035028, 2010.
[24] V. Thakar, Z. Wu, and M. Rais-Zadeh, "A high ON/OFF ratio MEMS capacitive switch with applications in solar energy harvesting," in *Proc. Solid-State Sens. Actuators, Microsyst. Workshop*, Hilton Head, SC, USA, 2012, pp. 385–388.
[25] Z. J. Yao, S. Chen, S. Eshelman, D. Denniston, and C. Goldsmith, "Micromachined low-loss microwave switches," *J. Microelectromech. Syst.*, vol. 8, no. 2, pp. 129–134, 1999.
[26] B. Lacroix *et al.*, "Sub-microsecond RF MEMS switched capacitors," *IEEE Trans. Microw. Theory Techn.*, vol. 55, no. 6, pp. 1314–1321, Jun. 2007.
[27] J. Park, E. S. Shim, W. Choi, Y. Kim, Y. Kwon, and D.-I. Cho, "A non-contact-type RF MEMS switch for 24-GHz radar applications," *J. Microelectromech. Syst.*, vol. 18, no. 1, pp. 163–173, Feb. 2009.
[28] M. Kaynak *et al.*, "BEOL embedded RF-MEMS switch for mm-wave applications," in *IEDM Tech. Dig.*, Dec. 2009, pp. 1–4.
[29] S. Fouladi and R. R. Mansour, "Capacitive RF MEMS switches fabricated in standard 0.35-μm CMOS technology," *IEEE Trans. Microw. Theory Techn.*, vol. 58, no. 2, pp. 478–486, Feb. 2010.
[30] R. Mahameed and G. M. Rebeiz, "A high-power temperature-stable electrostatic RF MEMS capacitive switch based on a thermal buckle-beam design," *J. Microelectromech. Syst.*, vol. 19, no. 4, pp. 816–826, Aug. 2010.
[31] M. Kaynak *et al.*, "BiCMOS embedded RF-MEMS switch for above 90 GHz applications using backside integration technique," in *IEDM Tech. Dig.*, Dec. 2010, pp. 5–36.
[32] R. Mahameed and G. M. Rebeiz, "RF MEMS capacitive switches for wide temperature range applications using a standard thin-film process," *IEEE Trans. Microw. Theory Techn.*, vol. 59, no. 7, pp. 1746–1752, Jul. 2011.
[33] R. K. Gupta and S. D. Senturia, "Pull-in time dynamics as a measure of absolute pressure," in *Proc. IEEE 10th Annu. Int. Micro Electro Mech. Syst. (MEMS)*, Jan. 1997, pp. 290–294.
[34] S. Shekhar, K. J. Vinoy, and G. K. Ananthasuresh, "Switching and release time analysis of electrostatically actuated capacitive RF MEMS switches," *Sens. Transducers*, vol. 130, no. 7, pp. 77–90, 2011.
[35] K. S. Chen and K. S. Ou, "Command-shaping techniques for electrostatic MEMS actuation: Analysis and simulation," *J. Microelectromech. Syst.*, vol. 16, no. 3, pp. 537–549, Jun. 2007.
[36] M. F. Daqaq, C. K. Reddy, and A. H. Nayfeh, "Input-shaping control of nonlinear MEMS," *Nonlinear Dyn.*, vol. 54, nos. 1–2, pp. 167–179, 2008.
[37] K.-S. Chen, T.-S. Yang, K.-S. Ou, and J.-F. Yin, "Design of command shapers for residual vibration suppression in Duffing nonlinear systems," *Mechatronics*, vol. 19, no. 2, pp. 184–198, 2009.
[38] S. Shekhar, K. J. Vinoy, and G. K. Ananthasuresh, "Design, fabrication and characterization of capacitive RF MEMS switches with low pull-in voltage," in *Proc. IEEE Int. Microw. RF Conf. (IMaRC)*, Dec. 2014, pp. 182–185.

Sudhanshu Shekhar received the M.S. degree from the University of Jamia Millia Islamia, New Delhi, India, in 2002; the M.Tech. degree from Panjab University, Chandigarh, India, in 2005; and the Ph.D. degree from the Centre for Nano Science and Engineering, Indian Institute of Science, Bengaluru, India, in 2016. He was a Lecturer at Jamia Millia University in 2006 and Amity University from 2006 to 2007. He is currently a Post-Doctoral Research Associate with the Department of Mechanical Engineering, Indian Institute of Science. His research interests include modeling, fabrication, and characterization of MEMS/RF MEMS devices and their reliability analysis, and microfabrication of micro devices for bio-medical applications.

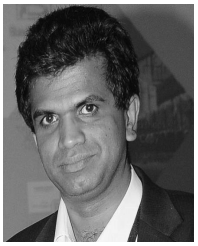

K. J. Vinoy (M'99) received the B.S. degree from the University of Kerala, Thiruvananthapuram, India, in 1990; the M.S. degree from the Cochin University of Science and Technology, Cochin, India, in 1993; and the Ph.D. degree from Pennsylvania State University, University Park, in 2002. He was a Research Assistant at the Center for Engineering of Electronics and Acoustic Materials and Devices, Pennsylvania State University, from 1999 to 2003. He is currently a Professor with the Department of Electrical Communication Engineering, Indian Institute of Science, Bengaluru, India. He has published over 150 papers in technical journals and conference proceedings. He has authored five books and four patents; one granted (U.S.) and three pending (India). His research interests include microwave antennas, microwave circuits, computational electromagnetics, and micro and nano technology applications (phase shifters, switches, and sensing circuits). He is also a fellow of the Indian National Academy of Engineers.

G. K. Ananthasuresh received the B.Tech. degree from IIT Madras, Chennai, India, in 1989; the M.S. degree from the University of Toledo, Toledo, OH, USA, in 1991; and the Ph.D. degree from the University of Michigan, Ann Arbor, MI, USA, in 1994. He was a Post-Doctoral Associate at the Massachusetts Institute of Technology, Cambridge, MA, USA; an Associate Professor at the University of Pennsylvania, Philadelphia, PA, USA; and a Visiting Professor at the University of Cambridge, Cambridge, U.K., and Katholike Univesiteit, Leuven, Belgium. He is currently a Professor of Mechanical Engineering and the Chair of Bio Systems Science and Engineering with the Indian Institute of Science, Bengaluru, India. He has co-authored 200 papers in journals and conferences, and two edited books, one text book, and 12 book-chapters. He has eight patents; four granted and four pending. His current research interests include compliant mechanisms, kinematics, multi-disciplinary design optimization, microsystems technology, micro- and meso-scale manufacturing technology, protein design, micromanipulation, and bio-design. He was a recipient of the NSF Career Award and the Ralph O. Teeter Educational Award in the USA, and the Swarnajayanthi Fellowship and the Shanti Swarup Bhatnagar Prize in India. He served on the editorial boards of eight journals.